Tunable Naphthalimide/Cinnoline-Fused (CinNapht) Hybrid Dyes for Fluorescence Imaging in Living Cells

Minh-duc Hoang, Farah Savina, Philippe Durand, Pr. Rachel Méallet-Renault, Gilles Clavier, Arnaud Chevalier

RESEARCH ARTICLE

Tunable Naphthalimide/Cinnoline-Fused (CinNapht) Hybrid Dyes for Fluorescence Imaging in Living Cells

Dr. Minh-Duc Hoang,[a] Farah Savina,[b] Dr. Philippe Durand,[a] Pr. Rachel Méallet-Renault,[b] Dr. Gilles Clavier,[c] and Dr. Arnaud Chevalier* [a]

[a] Université Paris-Saclay, CNRS, Institut de Chimie des Substances Naturelles, UPR 2301, 91198, Gif-sur-Yvette, France. E-mail: arnaud.chevalier@cnrs.fr
[b] Université Paris-Saclay, CNRS, Institut des Sciences Moléculaires d'Orsay, Orsay,91405, France
[c] Université Paris-Saclay, ENS Paris-Saclay, CNRS, PPSM, 91190, Gif-sur-Yvette, France

Supporting information for this article is given via a link at the end of the document

Abstract: This paper presents the synthesis, photophysical characterization and use for cell imaging of 14 flurophores derived from a hybrid Naphthalimide/Cinnoline fused backbone called "CinNapht". Photophysical properties of these fluorophores including absorbance, excitation and emission spectra have been recorded in $CHCl_3$, DMSO and PBS + 5%BSA. They exhibit red emission associated to a large Stokes Shift and fluorescence quantum yields up to 52%. Theoretical calculations have been undertaken in order to provide elements of rationalization for a major part of the results. Some of these analogues have been tuned to enable imaging of cell organelles such as mitochondria, lysosome or lipid droplets. This study comes to confirm that CinNapht dyes can be considered as relevant alternatives to existing tools for cell imaging.

Introduction

The synthesis of new organic fluorophores and the optimization of their photophysical properties has enabled the emergence of scaffolds endowed with a wide range of performances, contributing to the development of fluorescence imaging. The motivations connected to this can be multiple. It can be to modulate the absorption and emission wavelengths of the fluorophores,[1] to improve its solubility in biological medium,[2] to enhance its photostability[3] or to address a given cell compartment.[4] The increasing number of fluorophores that have been, and are still being proposed, demonstrates that the perfect fluorophore does not exist. Despite the wide variety of existing fluorophores, there is still a need for new tools to solve specific problems of fluorescence imaging.[5] The knowledge acquired since decades on the structure/photophysical properties relationship now enables to anticipate the consequences of functional adjustments to obtain fluorophores with optimized properties. For example, the nature of the amine substituents carried by the fluorophores significantly influences their emission properties and the fluorescence efficiency. This made possible the fine tuning of fluorophores photophysical properties, whether they are xanthene[6] or ICT involving structures.[7] In this context, combining a stokes shift enhancement with a redshift of the absorption and emission wavelengths is one of the most addressed topics.[8] Multiple approaches have been implemented for this purpose, as clearly explains by Yuan's group.[9] Possible approaches consist of either introducing alternating vibronic structures or extending the polyaromatic system's conjugation of existing structures, for example, by elaborating fused hybrid fluorophores. The latter strategy has already been implemented on multiple fluorophores including coumarins,[10] BODIPY's[11] or rhodamines[6a] being fused with either coumarin moiety[12] or cyanine dyes.[13] Efforts to develop fused hybrid fluorophores based on a naphthalimide structure have also been reported (Figure 1).[14]

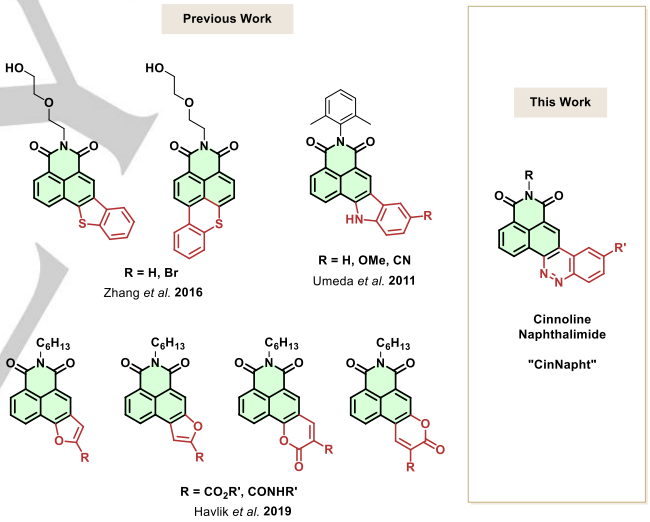

Figure 1. Previous work relating to hybride fused dyes incorporating a naphthalimide moiety.

Inspired by work describing "covalent-assembly" probes[15] resulting in the formation of cinnoline incorporating fluorophores,[16] we recently published the study of a fused hybrid structure involving a naphthalimide and a cinnoline, called CinNapht[17]. We showed that the extended conjugation of the Naphthalimides resulted in a bathochromic shift of the absorption and emission wavelengths of the fluorophores while preserving a high Stokes shift. In the present article, we describe a synthetic method that allowed structural adjustments on the CinNapht backbone (Figure 1). The specificity of these fluorophores lies in their easy modification at two distinct positions. We show that photophysical properties of the fluorophore can be modulated by changing the nature of a donor group (shown in blue, Scheme 1). Furthermore, we illustrate the utility of varying the substituent of the phthalimide moiety (Red R, Scheme 1) to provide cell organelles targeting ability to the fluorophore. This convergent

synthesis, involving coupling of functionalized naphthalimide and cinnoline moieties in the final steps, gives easy access to multiple combinations and therefore to a high diversity of fluorophores.

Results and Discussion

Synthesis of CinNapht Analogues.

The designed synthetic strategy for CinNapht **8** is based on Suzuki cross-coupling reaction between boronate **6** and 3-bromo-4-amino-N-substituted 1,8-naphthalimide **3** followed by intramolecular diazotization of the formed *ortho* amino biphenyl. derivatives **7**. The N-alkylated phthalimides **3** were synthesized in a two steps process from 4-amino-1,8-naphthyl anhydride as previously reported.[17]

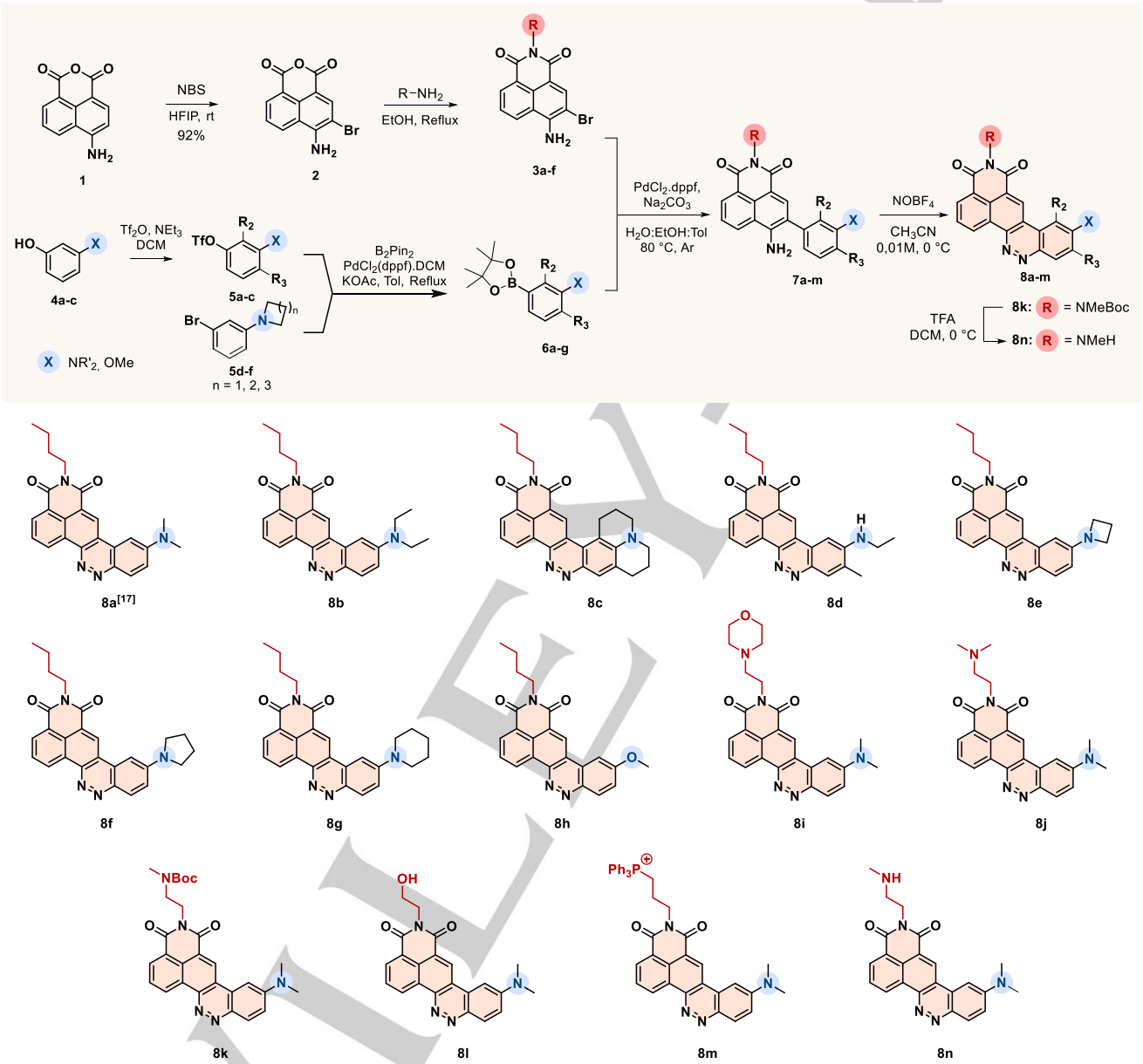

Scheme 1. Synthesis route and structure of CinNapht analogues.

The brominated intermediates **2** are easily isolated by precipitation and can react with various amines (Scheme 1), allowing the introduction of alkyl group R carrying alcohol (**3e**), Boc protected amine (**3d**) or triphenylphosphonium groups (**3c**) The obtained isolated yields vary from 68 to 99% (See Supporting Information for detailed protocols,). Note that these two steps can be interchanged if necessary, but resulting in lower overall yield. The boronic acid pinacol ester **6a-g**, second partners in the Suzuki cross-coupling reaction, were synthesized by palladium catalyzed coupling reaction of bis(pinacolato)diboron with either 3-bromo dialkylamino aryl **5d-f** or 3-dialkylamino aryl triflate **5a-c**. The latter were obtained from the corresponding phenol under standard conditions with good yields. These two possible precursors for **6** give access to CinNapht with various donor moieties, allowing their emission wavelength tuning. After Pd-catalyzed Suzuki coupling between boronate **6a-d** and

brominated naphthalimide **3a-f,** the bisaryl adduct **7a-n** can be obtained in up to 93% yield. At this step, purification on silica gel was necessary to provide a compound pure enough to ensure its easy and good yielding transformation into the CinNapht fluorophore **8a-n**. This last step consists in the formation of a diazonium salt using nitrosyl tetrafluoroborate that undergoes the internal addition of the aromatic ring through a SE_{Ar} type reaction. It must be noted here that this last step leads to a mixture of regioisomers resulting from *para* and *ortho* addition. Fortunately, under these conditions, the fluorescent *para*-substitution isomer was systematically found to be the major product. A set of 14 fluorophores was obtained through this synthetic route with multiple structures presented in Scheme 1.

Table 1. Photophysical properties of CinNaphts **8a-n** in different solvents at 25 °C

CinNapht Dye	Solvent	λ_{max} Abs[a] (nm)	ε_{max}[b] ($M^{-1}.cm^{-1}$)	λ_{max} Em (nm)	Stokes Shift (cm^{-1})	QY_{FL}[c]	Brightness[d]
8a	$CHCl_3$	489[e]	15 700[e]	566[e]	2 782[e]	0.25[e]	3 925[e]
	DMSO	496[e]	15 500[e]	682[e]	5 499[e]	0.06[e]	930[e]
	PBS + 5% BSA	518	11 879 ± 3 070	643	3 752	0.07	831
8b	$CHCl_3$	506	14 690 ± 1 232	575	2 371	0.26	3 819
	DMSO	505	13 952 ± 246	674	4 965	0.17	2 371
	PBS + 5% BSA	522	10 062 ± 1 575	642	3 580	0.08	804
8c	$CHCl_3$	535	7 215 ± 1 208	615	2 431	0.52	3 752
	DMSO	537	9 264 ± 1 144	704	4 417	0.13	1 204
	PBS + 5% BSA	544	2 431 ± 83	649	2 974	0.04	97
8d	$CHCl_3$	463	15 883 ± 620	560	3 741	0.19	3 017
	DMSO	483	9 249 ± 437	659	5 529	0.14	1 387
	PBS + 5% BSA	492	5 388 ± 301	620	4 196	0.05	269
8e	$CHCl_3$	484	13 066 ± 898	577	3 330	0.33	4 311
	DMSO	491	12 939 ± 463	696	5 998	0.09	1 164
	PBS + 5% BSA	501	3 424 ± 80	613	3 646	0.04	0.04
8f	$CHCl_3$	502	8 542 ± 1 419	572	2 438	0.29	2 477
	DMSO	504	11 613 ± 462	690	5 348	0.18	2 090
	PBS + 5% BSA	515	3 646 ± 165	612	3 078	0.04	145
8g	$CHCl_3$	485	7 539 ± 1 541	592	3 727	0.38	2 864
	DMSO	505	9 496 ± 661	691	5 330	0.08	759
	PBS + 5% BSA	518	2 827 ± 378	604	2 748	0.03	089
8h	$CHCl_3$	398	10 963 ± 1 681	n.d.	n.a.	n.a.	n.a.
	DMSO	421	9 323 ± 97	n.d.	n.a.	n.a.	n.a.
	PBS + 5% BSA	398	n.d[f]	n.d.	n.a.	n.a.	n.a.
8i	$CHCl_3$	487	14 165 ± 3 587	572	3 051	0.20	2 833
	DMSO	498	14 032 ± 199	696	5 712	0.07	982
	PBS + 5% BSA	505	7 498 ± 724	631	3 954	0.04	299
8j	$CHCl_3$	495	9 433 ± 729	586	3 137	0.23	2 169
	DMSO	499	10 612 ± 673	694	5 630	0.07	742
	PBS + 5% BSA	512	n.d[f]	627	3 582	< 0.01	n.a.
8k	$CHCl_3$	483	10 629 ± 914	568	3 098	0.21	2 232
	DMSO	491	9 877 ± 1 003	697	6 019	0.04	395
	PBS + 5% BSA	495	n.d[f]	611	3 835	< 0.01	n.a.
8l	$CHCl_3$	495	6 334 ± 854	585	3 108	0.21	1 330
	DMSO	496	10 635 ± 217	693	5 854	0.06	638
	PBS + 5% BSA	515	10 151 ± 1 561	648	3 985	0.03	304
8m	$CHCl_3$	487	7 142 ± 1 044	649	5 196	0.22	1 571
	DMSO	498	11 912 ± 360	698	5 754	0.09	1 072
	PBS + 5% BSA	518	7 664 ± 345	637	3 606	0.02	153
8n	$CHCl_3$	500	2 711 ± 498	602	3 389	0.20	542
	DMSO	499	5 800 ± 96	689	5 526	0.06	348
	PBS + 5% BSA	511	n.d[f]	685	4 970	< 0.01	n.a.

[a] Values corresponding to S_0-S_1 transition but strong S_0-S_2 transition is also observed (see Supporting Information Fig S1 to S17), [b] Molar extinction coefficient related to S_0-S_1 transition. [c] Relative QY determined at 25 °C using $[Ru(bpy)_3]Cl_2$ (QY = 0.04 in air Saturated H_2O), All compounds QY_{FI} were determined using excitation wavelength at 470 nm except for **8c** (λ_{Exc} = 490 nm) and compound **8d** (λ_{Exc} = 450 nm) [18] [d] Brightness was calculated using the formula: Brightness = $QY_{FI} \times \varepsilon_{max,}$ [e] Previously reported values[17], [f]. Poor solubility could not enable to obtain an accurate value.

Their chemical structure, as well as the synthetic intermediates compounds, were unambiguously confirmed by detailed measurements, including ESI-HRMS and NMR analyses (see Supporting Information). The CinNaphts from **8a** to **8h** constitute a set of fluorophores for which the *N*-butylphthalimide moiety was fixed and for which the substituents on the cinnoline moiety (blue in scheme 1) were modulated to allow photophysical tuning. On the other hand, for fluorophores **8i** to **8n**, the dimethylaniline donor moiety is kept unchanged to study the impact of a modification of the phthalimide moiety.

Photophysical properties

The photophysical properties of all these dyes were firstly evaluated in solution in chloroform and the results are presented in Table 1. No significant variation was observed in the absorption maxima by modifying the R substituent while keeping the donor part unchanged. Thus, CinNapht **8i-n** show similar absorption maxima fluctuating between 485 and 495 nm. On the other hand, the increased donor character of the cinnoline susbtituents causes a bathochromic shift of the absorption maxima. Thus compounds **8h**, **8d**, **8a**, **8b**, and **8c**, ranked according to the donor strength of their substituents, show an increasing trend of absorption maxima with values of 398, 463, 489, 506 and 535 nm respectively. More surprisingly, the substituent ring size in the case of CinNaphts **8e**, **8f** and **8g** also seems to impact the absorption maxima, although the donor character is not supposed to be taken into consideration in this case. The most remarkable impact on the absorbance was observed for the molar extinction coefficient. Among all the cyclic amines **8e-g** used as substituent, the azetidine provide the strongest increase of the ε. The same behavior was observed for the emission maxima with values of 560, 566, 575 and 615 nm for CinNaphts **8d**, **8a**, **8b**, and **8c** respectively. A surprisingly high emission wavelength was measured for the compound **8m** associated to a shoulder shaped emission spectrum (See Figure S12). We suppose that this might be due to some aggregation phenomenon, but no definitive explanation can be given at this stage. Note that for all the synthesized fluorophores, a large Stokes shift was observed with a lowest value of 2371 cm^{-1} (**8b**) which rises to 5196 cm^{-1} for CinNapht **8m**. This is a common consequence when fluorophores excited state is of an intramolecular charge transfer (ICT) nature.[17] Despite our efforts in trying to bring an explanation, in particular by calculation, we could not provide any element allowing to link the Stokes Shift values to the structure of the compounds in a rational way. Concerning the fluorescence quantum yield (QY_{Fl}), significant variations are to be noted. The use of a diethyl amine unit in CinNapht **8b** in place of the dimethyl amine analogue (**8a**) only results in a slight variation. In contrast, the introduction of the julolidine unit leads to a significant increase in the quantum yield to 52%. This can be explained by the prohibition of the rotation of the C-N bond, which could generate twisted forms that are often non-fluorescent.[19] Another meaningful result is the almost complete fluorescence extinction for compound **8h** with an alkoxy donor group, (QY_{Fl} < 0.1%). Although a partial decrease in fluorescence is widely reported in the literature, with this substituent, its complete disappearance is unusual. The graphical representation reported in Figure 2 clearly illustrates how modifying the donor part affects CinNaphts properties. For example, the introduction of a particularly donor group, such as julolidine, induces a pronounced bathochromic shift in both the absorption and emission spectra. This result is consistent with the literature, which has consistently supported the relevance of this group for shifting wavelengths to the red zone. Fluorescence quantum yields were measured around 20% to 30% and found homogenous for CinNaphts **8i-n** regardless of the nature of R substituting phthalimide moiety and the emission wavelength (Figure 2A). By contrast, the impact of the structural modifications on the brightness value was more evident (Figure 2B). Considering the poor variations observed in the QY_{Fl} values, we can assert that these variations are mostly related to molar extinction coefficients heterogeneity. Thus the most efficient fluorophore finally seems to be CinNapht **8e** which confirms once again the benefit of introducing an azetidine motif to improve the fluorophore's performance.[6c, 20] The Judolidine motif seems also convenient as proved by the acceptable brightness of CinNapht **8c** associated with a red-shifted emission.

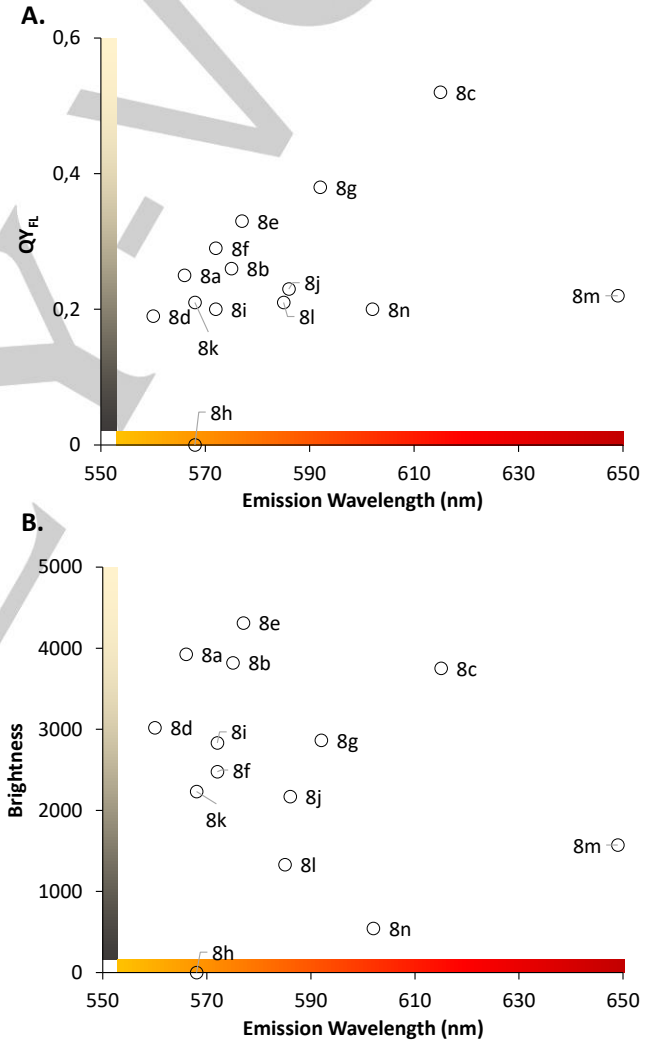

Figure 2. Graphical representation of photophysical properties heterogeneity of CinNapht **8a-n** at 25 °C in $CHCl_3$. **A:** Quantum Yield and Emission wavelength plot. **B:** Brightness and Emission wavelength plot.

In order to confirm the solvatochromism effect observed in the previous study[17], the photophysical properties of the compounds have also been investigated more polar solvents. The measurements in DMSO (Table 1) confirmed a systematic bathochromic shift of the emission wavelengths characterizing the ICT fluorophores showing a marked solvatochromism. Given the

small shift in absorbance wavelengths, this is also manifested by a significant increase in the Stokes shift which reaches high values up to 5 998 cm-1. Likewise in the previous study, we noticed a significant drop in the quantum yield. However, we could observe quite good fluorescence efficiency for some of the dyes including CinNapht **8b** (QY_{Fl} **=** 0.17) for the CinNapht **8d** (QY_{Fl} **=** 0.14) for which fluorescence quantum yields values were found to be two to three times higher than for the reference compound **8a**[17]. We also studied the fluorescence of these compounds in an aqueous medium. The fluorescence was extremely low in PBS buffer (data not shown), but a supplementation of the buffer with 5% BSA, in order to limit aggregation, allowed to observe more reliable fluorescence. The values presented in Table 1 show nevertheless a rather low fluorescence intensity that are probably resulting from a lack of solubility. Note that the epsilon values are very variable with respect to the solvent employed, with significantly lower values in PBS buffer. We have no concrete explanation at this stage of the study, although an aggregation phenomenon may be at the origin of these observed discrepancies.

TD-DFT Calculation

In order to rationalize the obtained experimental results, a series of quantum mechanical calculations has been undertaken. The very slight variation in absorption when the dimethylaniline donor moiety is kept unchanged is supported by theoretical calculation. We could indeed notice a quite constant HOMO-LUMO gap values observed for CinNaphts **8i** to **8h** (Figure S19). Note that the red-shifted absorption λ_{Max} of the CinNapht **8c** can also be explained by a smaller calculated value of HOMO-LUMO gap (Figure S19) as well as the increase of HOMO-LUMO gap calculated for compound **8d** can also explain the hypsochromic shift its absorbance wavelength.

Table 2. Comparison between experimental and theoretical results including oscillator strength (f)

CinNapht Dye	Absorption			Emission	
	λ_{max} Calc (nm)	Δ (Exp-Calc)	f	λ_{max} Calc (nm)	Δ (Exp-Calc)
8a	497	1,6 %	0.310	544	3,9 %
8b	491	3,0 %	0.321	549	4,5 %
8c	522	2,4 %	0.372	580	5,7 %
8d	470	1,5 %	0.335	521	7,0 %
8e	492	1,7 %	0.332	555	3,8 %
8f	506	0,8 %	0.322	555	3,0 %
8g	476	1,9 %	0.331	566	4,4 %
8h	396	0,5 %	0.401	/	/
8i	499	2,5 %	0.309	547	4,4 %
8j	499	0,8 %	0.307	563	3,9 %
8k	501	3,7 %	0.309	548	3,5 %
8l	501	1,2 %	0.305	548	6,3 %
8m	516	6,0 %	0.329	562	13,8 %
8n	498	0,4 %	0.310	546	9,3 %

All the structures have been optimized in their ground and first excited states by DFT followed by a TDDFT analysis of both states to obtain calculated transitions corresponding to absorption and emission respectively (Table 2).The calculated absorbance values are in good agreement with the experimentally generated data. We can observe only very small deviations of up to only 6%. These percentages tend to be higher when considering the emission. Nevertheless, consistency is observed in the trend of the bathochromic shift resulting from the increase of the donating character of the amine of CinNapht. Oscillator strengths vary between 0.3 and 0.4 which is quite consistent with transitions having intermediate molar absorption coefficients around 10 000-15 000.

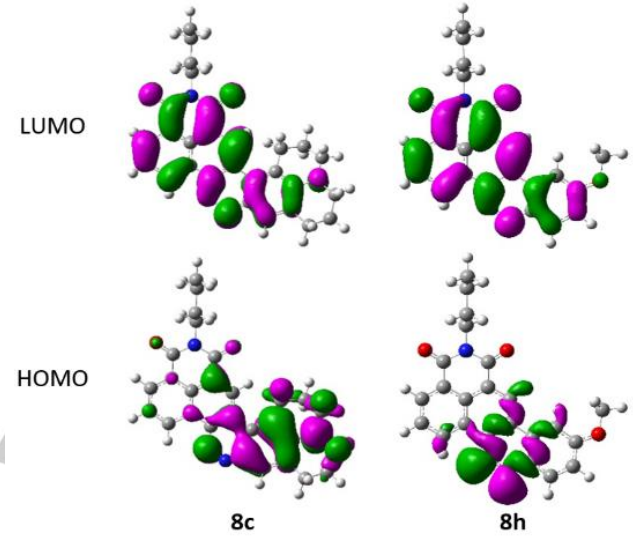

Figure 3. Left: frontiers molecular orbitals of **8c** which are representative of all compounds substituted by a nitrogen; right: frontiers molecular orbitals of **8h** in its first excited state geometry. Note the nature of the HOMO that is constituted by the lone pairs of the nitrogen atoms of the cinnoline.

All the compounds bearing a nitrogen substituent on the cinnoline moiety display a HOMO-LUMO π-π* transition that has a certain charge transfer character as can be seen from the orbitals representation (Figure 3 left). The calculations made on CinNapht **8h,** with a methoxy substituent, indicate that the relaxed S1 state is of a different nature since it corresponds to a n-π* transition (note the nature of the HOMO that is constituted by the lone pairs of the nitrogen atoms of the cinnoline in Figure 3 right). This major difference explains its poor emission properties.

Fluorescence Microscopy

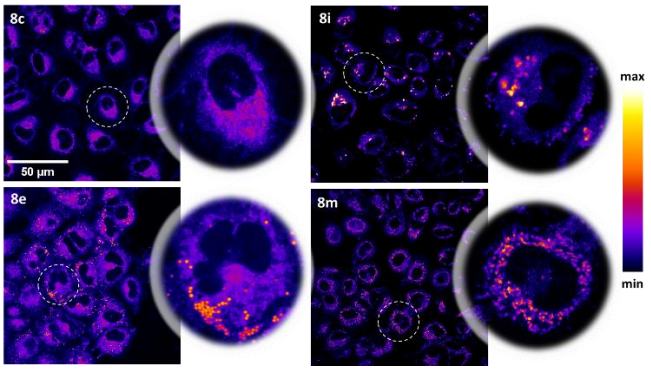

Figure 4. Confocal microscopic images of live A549 Cancer cells treated with compounds 8c, 8e, 8i and 8m (Exc: 490 nm, Em: 520–750 nm) 5 µM for 3 h at 37 °C using a 40x oil immersion objective.

A set of selected fluorophores were incubated in the presence of A549 lung cancer cells to evaluate their potential for fluorescence microscopy. We first examined the intracellular distribution of the

fluorescent CinNaphts **8c**, **8e**, **8i** and **8m**. The compounds were incubated for 3h at a concentration of 5 µM in live A549 lung cancer cell and then imaged with confocal microscopy (Figure 4). At first glance, we could rapidly notice that the intracellular biodistribution of these four fluorophores was significantly different. While compound **8c** does not seem to display any particular compartmentalization, compounds **8e**, **8i**, and **8m** are visibly localized in cellular compartments, suggesting respectively lipid droplets, lysosome, and mitochondria. These results were expected for CinNaphts **8i** and **8m,** carrying a morpholine and moiety triphenylphosphonium[21] moieties known to target lysosome[22] and mitochondria[23] respectively when attached to fluorophores including naphthalimides. On the other hand, the preferential accumulation of **8c** in lipid droplets was not initially expected. This being said, taking into account the fact that the solvatochromism usually characterizes ICT fluorophores, including our CinNaphts, is one of the prerequisites for the design of probes targeting these lipid droplets, it finally appears plausible to be capable of targeting these compartments with some of our analogs.[24] In order to confirm the observed subcellular compartmentalization, colocalization experiments were conducted.

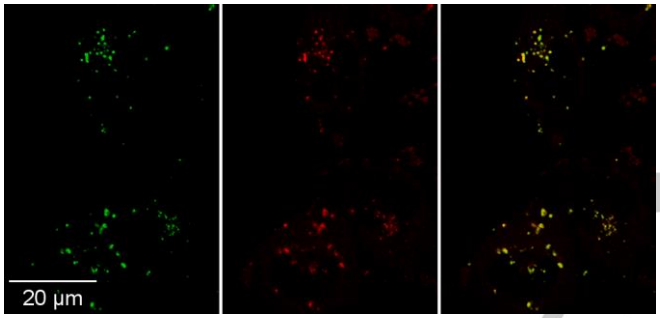

Figure 5. Confocal Mircoscopy Colocalization experiment with CinNapht **8i** (5µM) and LysoView™ 488 on A549 live cells. Left : LysoView™ 488 (λ_{Exc}: 480 nm, λ_{Em}: 500 to 530 nm), Middle: CinNapht **8i** (λ_{Exc} 488 nm, λ_{Em}: 600 to 700 nm), Right: Overlay.

The CinNapht **8i** was incubated for 3h at 5µM in A549 cells in the presence of a lysosome marker (LysoView™ 488) to validate its lysosomal localization (Figure 5). Results reveal a pronounced correlation between the red and green signals characterized by the appearance of yellow spots on the overlay shot. If it is evident that the signal peaks observed in the case of CinNapht **8i** match the signal of the lysosome, the noisy aspect of the signal highlight the imperfect lysosomal labeling. The cytofluorogram (Figure S20A) and the plot profile (Figure S20B) supported these preliminary observations. In addition, the control experiment performed with a mitochondrial marker (MitoView™ Green) shows a mismatch between the green and red signals (Figure S21). Together, these results confirms that the morpholine moiety enabeled the accumulation of the CinNapht **8i** in the lysosome. Similarly, we studied the mitochondrial localization of CinNapht **8m**. For this experiment, a MitoView™ Green was used, and the control experiment was performed with a LysoView™ 488. The images depicted in Figure 6 indicate a much more evident localization. These observations are validated by a cytofluorogramm (Figure S22A) showing pixels following the correlation line (Paearson Correlation Coefficient : 0.84) and a plot profile (Figure S22B) revealing a high degree of correlation between the green and red signals. By contrast, the control using the lysosome marker displayed a mismatch of the two signals (Figure S23).

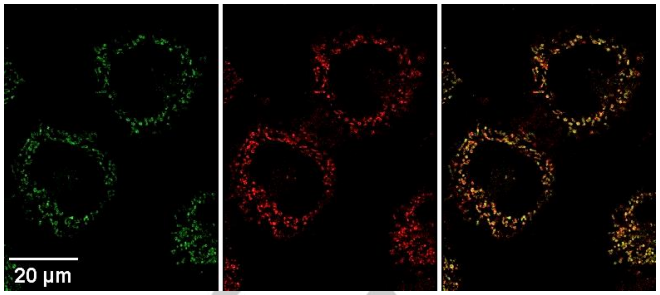

Figure 6. Confocal Mircoscopy Colocalization experiment with CinNapht **8m** (5µM) on A549 live cells and MitoView™ Green. Left : MitoView™ Green (λ_{Exc}: 480 nm, λ_{Em}: 500 to 530 nm), Middle: CinNapht **8m** (λ_{Exc} 488 nm, λ_{Em}: 600 to 700 nm), Right: Overlay.

All together, these results demonstrate that the functionalization of CinNapht with a triphenylphosphonium motif allows a very efficient targeting of the mitochondria.To complete the study, we also checked the localization of CinNapht **8e**. The fluorophore was incubated at 5 µM in A549 cells and a lipid droplet marker was added. The pictures displayed in Figure 7 show a strong correlation between the signal of **8e** and LipidSpot 610 thus confirming the preferential accumulation of CinNapht **8e** in lipid droplets.

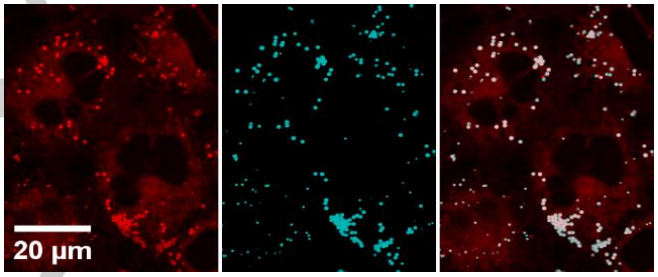

Figure 7. Confocal Mircoscopy Colocalization experiment with CinNapht **8e** (5µM) and LipidSpot™ 610 on A549 live cells. Left : CinNapht **8e** (λ_{Exc} 480 nm, λ_{Em}: 550 to 600 nm), Middle:, LipidSpot™ 610 (λ_{Exc}: 610 nm, λ_{Em}: 650 to 750 nm) Right: Overlay.

However, it is still evident that this fluorophore does not allow a specific visualization of these compartments because of the high signal observed in the rest of the cell. The CinNapht **8e** can however constitute an alternative tool for the visualization of these hydrophobic compartments in living cells. We evaluated the toxicity of the 4 compounds studied by microscopy (Figure S24). The CinNaphts **8c, 8i** and **8e** displayed no obvious toxicity after 72h of incubation, even at higher concentrations up to 10 times the concentration used for the microscopy experiments. On the other hand, compound 8m turned out to be quite toxic at 50 µM after 72h. Considering its low toxicity at 5µM after 72h of incubation, we can still consider it as compatible with imaging experiments for which the incubation time is much shorter.

Conclusion

To summarize, the synthetic route presented here allows to functionalize independently the two parts of the CinNapht fluorophores in order to link them together in a late stage of the synthesis. This method offers multiple combinations as illustrated by these 14 different fluorophores presented in this article including 13 undescribed analogues. Photophysical

measurments supported by theoretical calculation demonstrated the interest of structural adjustment of these CinNaphts in order to tune their optical properties. Fluorescence microscopy experiments revealed that the introduction of specific functions on the phthalimide moiety allows to vectorize these fluorophores in a given cell compartment such as mitochondria or the lysosome. This set of fluorophores, although not exhaustive, demonstrates the modularity of CinNapht dyes and how they can represent plausible alternative to existing tolls in both photophysical and biological purposes.

Experimental Section

Organic synthesis protocols

General procedure A (synthesis of brominated naphthalimides molecules 3a-f)

To a suspension of compound **1** (0.17 mmol, 1.00 eq.) in absolute ethanol (1.00 mL) was added the appropriate amine partner (0.34 mmol, 2.00 eq.). The reaction mixture was refluxed overnight. After the reaction was completed, the mixture was cooled down to room temperature and the resulting solid was isolated by filtration then washed with diethyl ether to furnish the desired brominated naphthalimide. The complete description of each compound including copy of NMR and MS spectra can be found in Supplementary Material.

General procedure B (synthesis of triflates 5a-c)

Trifluoromethanesulfonic anhydride (244 µL, 1.45 mmol, 1.10 eq.) was slowly added to a solution of appropriate phenol (1.32 mmol, 1.00 eq.) and triethylamine (220 µL, 1.58 mmol, 1.20 eq.) in anhydrous DCM (5.00 mL) at 0 °C. The reacting mixture was stirred under an argon atmosphere at 0 °C for 2 h. After the reaction was completed, 5.00 mL of a saturated NH_4Cl solution was added to quench the reaction. The reaction mixture was transferred to a separating funnel and the aqueous phase was removed. The organic phase was dried ($MgSO_4$), filtered, and concentrated under reduced pressure. The crude residue was purified by flash column chromatography on silica gel using an appropriate elution system to give the phenolic triflates **5a-c**. The complete description of each compound including NMR and MS spectra can be found in Supplementary Material.

General procedure C (synthesis of molecules 6a-f)

Compound **5** (1.00 eq.), bis(pinacolato)diboron (1.50 eq.) and KOAc (3.00 eq.) were dissolved in toluene (0.10M) in a Schlenk tube. The resulting mixture was deoxygenated with freeze-pump-thaw cycling before addition of $Pd(dppf)Cl_2$.DCM (0.10 eq.). The reaction was heated to 90 °C with constant stirring under argon for 17 h. The mixture was then cooled to room temperature, diluted with CH_2Cl_2 and washed with water. The organic phase was dried over $MgSO_4$, filtered, and concentrated under reduced pressure. The crude residue was purified by flash column chromatography on silica gel using an appropriate elution system to furnish pure pinacol borane esters **6a-f**. The complete description of each compound including copy of NMR and MS spectra can be found in Supplementary Material.

General procedure D (synthesis of molecules 7a-f):

Brominated naphthalimide analogue **3** (1.00 eq.), appropriate pinacol borane ester **6** (1.20 eq.), and Na_2CO_3 (3.00 eq.) were dissolved in a tertiary mixt of solvent composed of H_2O, EtOH, and toluene (v/v 3:3:10, 0.15M) in a Schlenk tube. The resulting mixture was deoxygenated with freeze-pump-thaw cycling before addition of $Pd(dppf)Cl_2$ (0.10 eq.). The reaction was heated to 80 °C with constant stirring under argon atmosphere for 17 h. The mixture was then cooled to room temperature, diluted with CH_2Cl_2 and washed with water. The organic layer was collected, dried over $MgSO_4$, and concentrated under reduced pressure. The crude residue was purified by flash column chromatography on silica gel using an appropriate elution system to give biaryl compounds **7a-f**. The complete description of each compound including NMR and MS spectra can be found in Supplementary Material.

General procedure E (synthesis of CinNaphts **8a-m**): A solution of compound **7** (1.00 eq.) in dry acetonitrile (0.01M) was cooled in an ice bath to 0 °C. Nitrosyl tetrafluoroborate (1.1 eq.) was added and the resulting reaction mixture was kept under stirring at 0 °C under and Argon atmosphere for 1 h. After the reaction was completed, the mixture was neutralized with as saturated $NaHCO_3$ solution and extracted with CH_2Cl_2. The organic layer was dried over $MgSO_4$ and concentrated under reduced pressure. The crude residue was purified by flash column chromatography on silica gel using an appropriate elution system. The complete description of each compound including copy of NMR and MS spectra can be found in Supplementary Material.

Photophysical Studies

UV-vis absorption measurements (scan mode) were conducted on a Shimadzu UV-visible spectrophotometer UV-2600 using rectangular 10 mm path length quartz cuvettes from Thuet, at 25 °C. Fluorescence spectroscopic studies (scan mode) were performed with a Fluoromax-4 spectrofluorometer (Jobin-Yvon; Horiba) at 25 °C, with rectangular 10 mm path length quartz cuvettes from Thuet. The absorption spectra were recorded with concentrations in the range 47-2.4 µM (total volume = 10 mL volumetric flask, six distinct dilutions for the accurate determination of molar extinction coefficients). The emission and excitation spectra were recorded with a diluted solution lower than 0.1 absorbance values. For the excitation and emission spectra the slits width were adjusted between 2-5 nm, integration time = 0.1 s, 1 nm step, HV (S1) = 950 V). All fluorescence spectra were corrected from the lamp fluctuations and the apparatus response fluctuations. Fluorescence quantum yields were measured at 25 °C, using three diluted solution (A<0.1) and three diluted solution of $Ru(bpy)_3^{2+}$ in air-saturated miliQ water (A<0.1). For each QY measurements, slidth width, excitation wavelength, scan rate, integration time and emission range were keep the same for the reference and the sample. The fluorescence quantum yield was determined thanks to the following formula:

$$\Phi F(x) = Sx/Ss(nX/nS)^2.\Phi F(s)$$

Where S is the slope of the linear plot of the integrated fluorescence intensity in function of the absorbance value, n is the refractive index of the solvents (at 25 °C) used in measurements, and the subscripts s and x represent standard and unknown, respectively.

The fluorescence quantum yield for the reference, $Ru(bpy)_3^{2+}$ in air-saturated miliQ water, was measured to be 0.040 in aerated water with the Horiba K-sphere accessory, in good correlation with the literature values.[18]

DFT Calculation

Ground state geometries were optimized at the B3LYP/6-31+g(d) level of calculation followed by a frequency calculation to confirm the convergence to a local minimum. TDDFT calculations were then done at the PBE0/6-311+g(d,p) level of theory to estimate absorption energies. Then first singlet excited state geometries were optimized at the PBE0/6-311+g(d,p) level followed by a frequency calculation at the same level. Finally, a TDDFT calculation was done on this S1 optimized geometries at the same level of theory to estimate the fluorescence emission wavelength. All calculations were done with Gaussian 16 (Revision B.01) software. Data were analyzed with GaussView 6.0 software

Cell culture and fluorescence Imaging

Cell lines were obtained from the American type Culture Collection (Rockville, USA) and were cultured according to the supplier's instructions. A459 cells were grown in RPMI 1640 containing 10% FCS and 1% glutamine. Cells were maintained at 37 °C in a humidified atmosphere containing 5% CO_2 and were split every 3 or 4 days at a time when enough confluence was obtained. An Ibidi® µ-Slide 8 Well high Glass Bottom plate was seeded with 10 000 cells/well and then maintained at 37 °C in a humidified atmosphere containing 5% CO_2 for 24h to 48h. After adequate confluence was obtained, the medium was removed and replaced by a solution of fluorophore at 5 µM in the appropriate medium, prepared from a stock solution of fluorophore in DMSO, final concentration in DMSO = 1.0%, please note that no solubility issue was noted). The cells were incubated for 3h at 37 °C in a humidified atmosphere containing 5% CO2. The fluorophofore solution was then removed and the cells were washed twice with pre-warmed PBS (1X). Finally, RPMI medium was added before imaging. (Procedures for organelle staining aiming colocalization experiments are given in Supporting Information)

Confocal fluorescence microscopy

Fluorescence images were acquired using a Leica SP8-X inverted confocal microscope with a 40× oil immersion objective (HC PL APO CS2 Leica). Excitation was performed using a White laser pulsed at 80MHz set at the desired excitation wavelength. Detection was carried out by using PMT detector (Hamamatsu 6357) collecting photons over the appropriate emission wavelength window. Recorded image size was 1024x1024 pixels and a pixel size of 65nm was reach using the zoom factor according sampling laws

Acknowledgements

This project has received funding by the French National Research Agency under the program CHARMMMAT ANR-11-LABX-0039-grant. This work was granted access to HPC resources from the “Mésocentre” computing center of CentraleSupélec and École Normale Supérieure Paris-Saclay supported by CNRS and Région Île-de-France (http://mesocentre.centralesupelec.fr/). We also thank the Institut de Chimie des Subtances Naturelles for their financial support. We also thank the pharamaceutical compunds screening plateform (CIBI Plateform) for their advices and technical support. The present work has benefited from Imagerie-Gif light microscopy core facility supported by French National Research Agency (ANR-11-EQPX-0029/Morphoscope, ANR-10-INBS-04/ FranceBioImaging; ANR-11-IDEX-0003-02/Saclay Plant Sciences). We thanks the Région Ile-de-France and DIM NanoK for financial support. The University Paris-Saclay and the CNRS are acknowledged for funding.

Keywords: Fluorophore • Naphthalimide • Cinnoline • Fluorescence Imaging • TD-DFT •

[1] aL. D. Lavis, R. T. Raines, *ACS Chem. Biol.* **2014**, *9*, 855-866; bL. D. Lavis, R. T. Raines, *ACS Chem. Biol.* **2008**, *3*, 142-155; cM. Ptaszek, in *Progress in Molecular Biology and Translational Science, Vol. 113* (Ed.: M. C. Morris), Academic Press, **2013**, pp. 59-108.

[2] X. Li, X. Gao, W. Shi, H. Ma, *Chem. Rev.* **2014**, *114*, 590-659.

[3] aA. N. Butkevich, M. L. Bossi, G. Lukinavičius, S. W. Hell, *J. Am. Chem. Soc* **2019**, *141*, 981-989; bJ. B. Grimm, L. Xie, J. C. Casler, R. Patel, A. N. Tkachuk, N. Falco, H. Choi, J. Lippincott-Schwartz, T. A. Brown, B. S. Glick, Z. Liu, L. D. Lavis, *JACS Au* **2021**, *1*, 690-696; cA. Rovira, M. Pujals, A. Gandioso, M. López-Corrales, M. Bosch, V. Marchán, *J. Org. Chem.* **2020**, *85*, 6086-6097; dJ. H. M. van der Velde, J. Oelerich, J. Huang, J. H. Smit, A. Aminian Jazi, S. Galiani, K. Kolmakov, G. Gouridis, C. Eggeling, A. Herrmann, G. Roelfes, T. Cordes, *Nat. Commun.* **2016**, *7*, 10144.

[4] aW. Xu, Z. Zeng, J.-H. Jiang, Y.-T. Chang, L. Yuan, *Angew. Chem. Int. Ed.* **2016**, *55*, 13658-13699; bH. Zhu, J. Fan, J. Du, X. Peng, *Acc. Chem. Res.* **2016**, *49*, 2115-2126; cJ. Lin, K. Yang, E. J. New, *Org. Biomol. Chem.* **2021**, *19*, 9339-9357.

[5] J. B. Grimm, L. D. Lavis, *Nat. Methods* **2022**, *19*, 149-158.

[6] aL. Wang, W. Du, Z. Hu, K. Uvdal, L. Li, W. Huang, *Angew. Chem. Int. Ed.* **2019**, *58*, 14026-14043; bJ. B. Grimm, A. N. Tkachuk, L. Xie, H. Choi, B. Mohar, N. Falco, K. Schaefer, R. Patel, Q. Zheng, Z. Liu, J. Lippincott-Schwartz, T. A. Brown, L. D. Lavis, *Nat. Methods* **2020**, *17*, 815-821; cJ. B. Grimm, A. K. Muthusamy, Y. Liang, T. A. Brown, W. C. Lemon, R. Patel, R. Lu, J. J. Macklin, P. J. Keller, N. Ji, L. D. Lavis, *Nat. Methods* **2017**, *14*, 987-994.

[7] aJ. Zhou, X. Lin, X. Ji, S. Xu, C. Liu, X. Dong, W. Zhao, *Org. Lett.* **2020**, *22*, 4413-4417; bA. Samanta, R. W. Fessenden, *J. Phys. Chem. A* **2000**, *104*, 8577-8582.

[8] aA. Rovira, M. Pujals, A. Gandioso, M. Lopez-Corrales, M. Bosch, V. Marchan, *J. Org. Chem.* **2020**, *85*, 6086-6097; bX. Ren, F. Zhang, H. Luo, L. Liao, X. Song, W. Chen, *Chem. Commun.* **2020**, *56*, 2159-2162; cX. Ren, F. Zhang, H. Luo, L. Liao, X. Song, W. Chen, *Chem. Commun.* **2020**, *56*, 2159-2162; dM. Mas-Montoya, M. F. Montenegro, A. Espinosa Ferao, A. Tarraga, J. N. Rodriguez-Lopez, D. Curiel, *Org. Lett.* **2020**, *22*, 3356-3360.

[9] T.-B. Ren, W. Xu, W. Zhang, X.-X. Zhang, Z.-Y. Wang, Z. Xiang, L. Yuan, X.-B. Zhang, *J. Am. Chem. Soc* **2018**, *140*, 7716-7722.

[10] M. Sarmah, K. Chutia, D. Dutta, P. Gogoi, *Org. Biomol. Chem.* **2022**, *20*, 55-72.

[11] aF. Ceugniet, Q. Huaulmé, A. Sutter, D. Jacquemin, N. Leclerc, G. Ulrich, *Chem. Eur. J.* **2022**, *n/a*, e202200130; bM. Khelladi, C. Maret, A. De Nicola, G. Ulrich, *Dyes and Pig.* **2022**, *198*; cT. Nakano, A. Sumida, K. Naka, *J. Org. Chem.* **2021**, *86*, 5690-5701; dJ. Wang, N. Boens, L. Jiao, E. Hao, *Org. Biomol. Chem.* **2020**, *18*, 4135-4156; eL.

Jean-Gérard, W. Vasseur, F. Scherninski, B. Andrioletti, *Chem. Commun.* **2018**, *54*, 12914-12929.

[12] aY. Yu, J. Wang, H. Xiang, L. Ying, C. Wu, H. Zhou, H. Liu, *Dyes and Pig.* **2020**, *183*; bJ. Chen, W. Liu, B. Zhou, G. Niu, H. Zhang, J. Wu, Y. Wang, W. Ju, P. Wang, *J. Org. Chem.* **2013**, *78*, 6121-6130; cA. Chevalier, P.-Y. Renard, A. Romieu, *Chem. Eur. J.* **2014**, *20*, 8330-8337.

[13] aH. Chen, W. Lin, H. Cui, W. Jiang, *Chem. Eur. J.* **2015**, *21*, 733-745; bL. Yuan, W. Lin, Y. Yang, H. Chen, *J. Am. Chem. Soc.* **2012**, *134*, 1200-1211; cL. Yuan, W. Lin, S. Zhao, W. Gao, B. Chen, L. He, S. Zhu, *J. Am. Chem. Soc.* **2012**, *134*, 13510-13523.

[14] aR. Umeda, H. Nishida, M. Otono, Y. Nishiyama, *Tetrahedron Lett.* **2011**, *52*, 5494-5496; bL. Zhang, K. Lei, J. Zhang, W. Song, Y. Zheng, S. Tan, Y. Gao, Y. Xu, J. Liu, X. Qian, *MedChemComm* **2016**, *7*, 1171-1175; cM. Havlik, V. Talianova, R. Kaplanek, T. Briza, B. Dolensky, J. Kralova, P. Martasek, V. Kral, *Chem. Commun.* **2019**, *55*, 2696-2699.

[15] aX. Luo, L. Gu, X. Qian, Y. Yang, *Chem. Commun.* **2020**, *56*, 9067-9078; bY. Yang, S. K. Seidlits, M. M. Adams, V. M. Lynch, C. E. Schmidt, E. V. Anslyn, J. B. Shear, *J. Am. Chem. Soc* **2010**, *132*, 13114-13116.

[16] aX. Lv, Y. Wang, S. Zhang, Y. Liu, J. Zhang, W. Guo, *Chem. Commun.* **2014**, *50*, 7499-7502; bY. Shen, Q. Zhang, X. Qian, Y. Yang, *Anal. Chem.* **2015**, *87*, 1274-1280; cC. G. Dai, J. L. Wang, Y. L. Fu, H. P. Zhou, Q. H. Song, *Anal. Chem.* **2017**, *89*, 10511-10519; dH. Zhang, X. Zhu, Y. Wang, Lanzhou University, Peop. Rep. China; Lanzhou University Zhongwei High-tech Research Institute . **2017**, p. 18pp; eX. Zhu, J. Q. Chen, C. Ma, X. Liu, X. P. Cao, H. Zhang, *Analyst* **2017**, *142*, 4623-4628; fP. R. Escamilla, Y. Shen, Q. Zhang, D. S. Hernandez, C. J. Howard, X. Qian, D. Y. Filonov, A. V. Kinev, J. B. Shear, E. V. Anslyn, Y. Yang, *Chem. Sci.* **2020**, *11*, 1394-1403.

[17] M.-D. Hoang, J.-B. Bodin, F. Savina, V. Steinmetz, J. Bignon, P. Durand, G. Clavier, R. Méallet-Renault, A. Chevalier, *RSC Adv.* **2021**, *11*, 30088-30092.

[18] K. Suzuki, A. Kobayashi, S. Kaneko, K. Takehira, T. Yoshihara, H. Ishida, Y. Shiina, S. Oishi, S. Tobita, *Phys. Chem. Chem. Phys.* **2009**, *11*, 9850-9860.

[19] aI. Ismail, D. Wang, Z. Wang, D. Wang, C. Zhang, L. Yi, Z. Xi, *Dyes and Pig.* **2019**, *163*, 700-706; bQ. Sun, S.-H. Yang, L. Wu, W.-C. Yang, G.-F. Yang, *Anal. Chem.* **2016**, *88*, 2266-2272.

[20] J. B. Grimm, B. P. English, J. Chen, J. P. Slaughter, Z. Zhang, A. Revyakin, R. Patel, J. J. Macklin, D. Normanno, R. H. Singer, T. Lionnet, L. D. Lavis, *Nat. Methods* **2015**, *12*, 244-250.

[21] aR. A. J. Smith, C. M. Porteous, A. M. Gane, M. P. Murphy, *Proc. Natl. Acad. Sci. U. S. A.* **2003**, *100*, 5407-5412; bJ. Zielonka, J. Joseph, A. Sikora, M. Hardy, O. Ouari, J. Vasquez-Vivar, G. Cheng, M. Lopez, B. Kalyanaraman, *Chem. Rev.* **2017**, *117*, 10043-10120.

[22] aJ. Zhou, W. Shi, L. Li, Q. Gong, X. Wu, X. Li, H. Ma, *Anal. Chem.* **2016**, *88*, 4557-4564; bJ. Zhou, W. Shi, L.-H. Li, Q.-Y. Gong, X.-F. Wu, X.-H. Li, H.-M. Ma, *Chem. Asian J.* **2016**, *11*, 2719-2724; cW. Hua, J. Zhao, X. Wang, S. Pei, S. Gou, *Analyst* **2019**, *144*, 6681-6688; dQ. Qiao, M. Zhao, H. Lang, D. Mao, J. Cui, Z. Xu, *RSC Adv.* **2014**, *4*, 25790-25794.

[23] aZ. Zhang, J. Fan, Y. Zhao, Y. Kang, J. Du, X. Peng, *ACS Sens.* **2018**, *3*, 735-741; bH.-W. Liu, S. Xu, P. Wang, X.-X. Hu, J. Zhang, L. Yuan, X.-B. Zhang, W. Tan, *Chem. Commun.* **2016**, *52*, 12330-12333; cZ. Wu, X. Tang, *Anal. Chem.* **2015**, *87*, 8613-8617.

[24] aM. Collot, S. Bou, T. K. Fam, L. Richert, Y. Mely, L. Danglot, A. S. Klymchenko, *Anal. Chem.* **2019**, *91*, 1928-1935; bT. K. Fam, A. S. Klymchenko, M. Collot, *Materials* **2018**, *11*; cA. H. Ashoka, P. Ashokkumar, Y. P. Kovtun, A. S. Klymchenko, *J. Phys. Chem. Lett.* **2019**, *10*, 2414-2421.

Entry for the Table of Contents

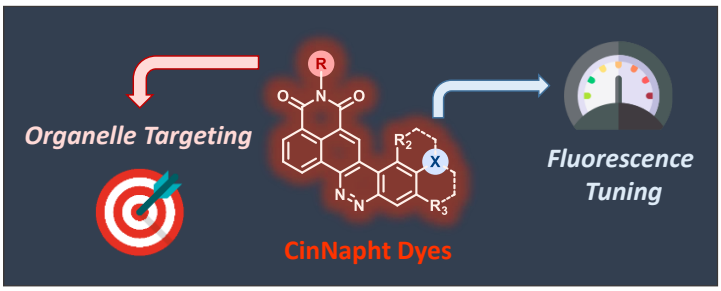

The versatile synthesis, photophysical characterization and use of multiple Cinnoline/Naphthalimide fused hybrid fluorophores for live cell imaging provides a comprehensive overview of “CinNapht” potential as bio-imaging agent.